

METHODS FOR THE DESIGN OF ENERGY EFFICIENT HIGH-SPEED AEROSPACE VEHICLES

Dr. David Riggins
University of Missouri – Rolla

Dr. David Moorhouse
United States Air Force Research Laboratory

Mr. Trent Taylor
University of Missouri – Rolla

Mr. Levi Terhune
University of Missouri - Rolla

Abstract

This paper continues development of the fundamental analytical science, methodology and tools required for the analysis, design, and optimization of high speed aerospace vehicles in terms of the efficient use of on-board energy. Specifically, it presents the complete second-law characterization and related system-level energy management effectiveness for high-speed vehicles (coupling both aerodynamic and propulsive subsystems). Modeling of the fluid dynamics utilizes high-level (multi-dimensional) flow-fields representative of generic configurations of interest. Capability has been recently developed which allows detailed second-law performance audits in terms of the ‘common currency’ of entropy generation for high-speed vehicles (involving complete synthesis of both internal and external flow-fields, i.e. both aerodynamic and propulsive sub-systems). This capability is now extended to encompass and utilize multi-dimensional flow-fields generated by computational fluid dynamics solvers, including Navier-Stokes solvers. Furthermore, the methodology is shown in this paper to provide insight and fundamental direction for management of on-board energy (‘price paid’) for maximum performance missions.

Nomenclature

C_p = specific heat at constant pressure
 F_x = net overall fluid-dynamic force component on vehicle in flight direction, N
 h = enthalpy per mass (J/kg)

H_{prop} = heating value of propellant (J/kg)
 M = Mach number
 \dot{m} = mass flow rate, kg/sec
 mw = molecular weight, kg/kmol
 P = static pressure, N/m²
 \dot{Q} = heat rate, J/sec
 R = gas constant, J/kg-K
 \dot{S} = entropy flow rate, J/K-sec
 T = static temperature, K
 ρ = static density, kg/m³
 \vec{V} = velocity vector, m/sec
 u,v,w = x,y,z Cartesian velocity components, m/sec
 \dot{W} = work rate, J/sec
 α_i = species mass fraction
 η_i = species mole fraction

Subscripts

$i,0$ = vehicle leading edge plane, free-stream
 e = vehicle exit plane
 inj = associated with propellant injection
 irr = irreversible processes
 l = species mass fraction
 $prop$ = propellant
 rev = reversible processes
 veh = associated with vehicle (propulsion/aerodynamics/sub-systems)
 w = wake exit plane
 $w,wake$ = wake process

1 Introduction

The design and engineering of aerospace vehicle systems for atmospheric flight at hypersonic Mach numbers will result in a dramatic expansion in the existing envelope of aerospace missions and mission feasibility. Such systems

will enable true global reach in terms of both military and civilian aircraft operations, redefine tactics and strategies of war-fighting operations, and enable faster, reliable, and less expensive space access. However, this capability also represents a formidable technical challenge in terms of the basic science, engineering, and operation of such vehicles. The hypersonic regime for powered flight is defined by extremes; these extremes are or will be experienced through vehicle stability and control, heat transfer, shock interactions and aerodynamic loads on vehicle structures, and finally the fluid dynamics and loss characteristics associated with the aero/propulsion subsystems of the vehicle. The fluid dynamics ultimately involves all other subsystems on the (energy-balanced) vehicle since the fluid in the aero/propulsion flow-paths serves as the final heat sink due to the generation of irreversibilities in all on-board sub-systems. In this sense, the fluid dynamics must ultimately be considered in any complete thermodynamic/sub-system analysis. Certainly the most obvious and limiting fluid dynamic result of the extremes associated with hypersonic (powered) flight is the well-known vanishingly small thrust – drag performance margins available for vehicles using current design paradigms.

The performance of hypersonic vehicles is largely governed by the degree with which the on-board energy can be most effectively transferred into useful aero-propulsive work. This useful work from the standpoint of the aero/propulsion context is entirely realized by driving the vehicle forward through the air in order to generate lift and side forces and axial and vertical accelerations as needed or desired. The effectiveness of how well this process is done is, in turn, inarguably and *always* related to the production of entropy through the entire system. (Entropy generation is most usefully associated with the rate at which work potential is being destroyed. In fact, the local entropy production simply scales with work potential lost by the inverse of the temperature at which the loss due to irreversibility occurs.) ***Note that entropy production is therefore the natural and***

fundamental measure of losses at all levels and across all subsystems. However, historically, entropy has not been utilized in the evaluation of either subsystems, components, or the overall vehicle in any more than in a passive fashion, i.e. as a kind of post-processed ‘curiosity’. Current sub-system, component, and indeed overall vehicle design instead rely on a relatively complex medley of efficiency and effectiveness factors which are to a greater or lesser degree related to entropy – however the relationships are often obscure or not explicitly called out. The fact that these factors usually work quite well is inarguable, since there is generally an enormous amount of engineering knowledge, sense and history built into them. For instance, total pressure is routinely used by propulsion engineers – changes in that quantity are indeed intimately related to entropy generation (irreversibility) as well as work interactions, however, the relationship is seldom noted or utilized (or even understood) by the practicing engineer.

The work discussed here is part of a larger effort (see Moorhouse [1]) directed at bringing entropy generation and analysis into the mainstream as the common currency of losses in engineering systems, specifically in terms of high-speed vehicle (and vehicle sub-system and component) design, analysis, evaluation, and optimization. Recent related work has provided entropy-based concepts and methodologies which allow the thermodynamic auditing of entire vehicle performance (Riggins [2]). These methodologies (which are streamtube based) originated in engine analysis but have been readily and rigorously extended to entire vehicle aero/propulsion systems. In addition, analytical work has related entropy production across both vehicle and wake to the force-based performance characterization of the vehicle. This analysis has pointed to the irreversibility which occurs in the wake as a critical part of the measure (note, not the cause) of the performance which actually happened over the vehicle. The analysis of this relationship between vehicle performance and entropy generation (reviewed in the second part of this paper) in fact provides the framework for the

multi-dimensional examples and analysis discussed at length in this paper.

Traditional design methodologies for both air-breathing and rocket-powered hypersonic vehicles are usually based on the premise that all on-board energy available in the aero/propulsion sub-systems should be added to the flow in the combustor, usually in terms of chemical heat release associated with fuel/oxidizer reaction. In terms of the basic thermal efficiency of a single system (the propulsion flowpath), this would certainly appear to be correct. In the combustor, pressures and temperatures are higher, and Mach numbers are lower. This translates into lower losses, i.e. lower entropy generation, when the energy is added to the flow. This lower entropy generation then leads to a more efficient vehicle, in terms of maximizing thrust or minimizing fuel used. However, when the perspective is broadened to include the entire vehicle, i.e. to include external aerodynamics as well as the propulsive flow-path, a significant potential exists for increasing the performance of the vehicle itself by considering 'distributed' energy schemes between external aerodynamics and propulsion (see Fig. 1 below). The use and tailoring of energy management in this fashion mandates understanding of the second-law characteristics of such non-conventional systems, either for components within given subsystems or for entire vehicles. It is specifically desired here to define and illustrate these ideas using relevant concepts and examples.

Early work done in the general area of losses in aerospace systems includes that of Foa [3] who sketched the characterization of performance system thrust and propulsive losses in terms of entropy rise across a jet engine (for matched pressure across the engine and other simplifying assumptions); he termed this the 'entropy method'. This is similar to the more general work of Riggins [4] who recently examined the thermodynamic spectrum of gas turbine engine performance from the standpoint of overall heat added, irreversibility (entropy

production), and work exchange in the propulsive flowpath. Lewis [5] provided clarification regarding the role of the second law in providing a universal definition of the propulsive efficiency for an isolated engine. The concept of thrust or thrust-work potential (also called stream-thrust based methods) for the performance characterization of high-speed ramjet and scramjet engines were first articulated by Curran and Craig [6]; considerable extension of their seminal work has been performed by Riggins, et al. [7]-[8]. The use of these methods has enabled the complete characterization of the loss in scramjet engine thrust due to irreversibility and has allowed the assessment of engine thrust losses in terms of irreversible loss mechanism and location. In a closely related development, the general concept of work availability as applied to aerospace jet engines (turbojets and turbofans) has been developed and utilized by Roth [9] – [10] who has suggested the use of work availability as a 'common currency' for engine design, evaluation, and optimization, generally without explicit consideration of entropy (second-law considerations) necessary. In addition, a significant amount of work has also been done in the area of applying conventional exergy (or availability) to the problem of aerospace vehicle design and evaluation (see, for example Clarke and Horlock [11] and Czysz and Murthy [12]). Availability is based on the assessment of the maximum reversible work as measured from a dead state and is attractive as a 'single currency' candidate; i.e. it is well-established and has an excellent track record for cyclic ground-based systems such as power plants. However, Riggins [13]-[14] has shown problems with conventional availability when directly applied to very simple jet engine optimization problems and has suggested a modification of exergy (called engine-based exergy) which essentially unifies it with the stream thrust concepts discussed above. The complete relationship between availability, entropy, and overall vehicle performance is derived and discussed in

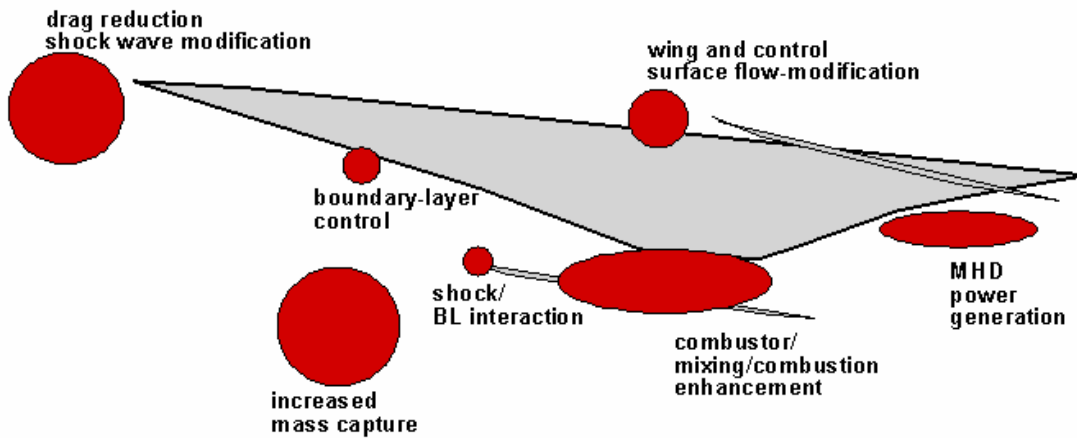


Fig. 1 Hypersonic vehicle: potential aero-propulsion on-board energy usage

the latter sections of this paper in which the critical importance of the vehicle wake mixing/equilibrium process is fully demonstrated.

The references listed above which detail previous/related work in the area of performance assessment are specific to the propulsion systems for flight vehicles. There has been significantly less work involving the development and use of entropy-based methods for external aerodynamic design, evaluation and optimization. An early reference which correctly incorporates the second law impact of the wake process for the drag on a base aerodynamic shape without energy interactions or mass addition is found in the textbook by Oswatitsch [15]. Giles and Cummings [16] provide an excellent discussion of the role of the wake in the assessment of vehicle drag. Greene [17] examined the role of entropy for induced drag minimization on low-speed airfoils using concepts related to this earlier work. Roth [18] – [19] have usefully extended work potential methods to a vehicle airframe with a turbine engine propulsion system and overall vehicle system loss management.

The first part of the work reported on here involves the ‘best use’ of on-board energy management as clarified via the entropy analysis for a relatively basic high-speed configuration. Specifically, a demonstration is

made of the dramatic reduction in external drag made possible on a simple hypersonic blunt body by the deposition of a minimal amount of energy upstream of the vehicle. This study is computational and uses two-dimensional CFD to generate the relevant flow-fields. When coupled with forward-facing injection of fuel, the upstream energy deposition results in jet stabilization. This interesting concept is clarified by second-law analysis in this work; it is a concept that (to a degree since the drag reduction for such a case has been observed and studied) reverses conventional wisdom that neither energy nor mass should be added *forward* of a vehicle. This observation is then further supported by a parametric (CFD) study of a simplified vehicle with an embedded rocket engine in which minimal on-board energy use required for cruise co-relates exactly with minimum generation of overall entropy in the flow-field.

Secondly, a parametric study is performed which examines the impact on vehicle performance of distributing energy between aero and propulsion subsystems on an *entire* air-breathing vehicle (external and internal propulsive flowpaths modeled using CFD). These results are again related to the entropy production via the analysis developed in this and other works. It is shown that maximum force-based performance is obtained when the available energy is appropriately distributed

between both propulsion flowpath (conventional) and the external aerodynamic flow-field. Specifically, the deposition of very small amounts of energy upstream of the vehicle and upstream and below the cowl is seen to be highly productive in generating less entropy production through and over the vehicle and in the wake mixing zone behind the vehicle.

2 Entropy and Vehicle Performance

The relationship between net aero/fluid-dynamic force in the direction of vehicle movement and entropy production and energy effects (see Fig. 2) has been described in a previous work [2]; for details of the derivation, see this reference. The powerful governing relationship which results in this analysis is given as:

$$\begin{aligned}
 F_x \cdot u_i &= \dot{Q}_{flow-path} + \dot{W}_{flow-path} + \dot{m}_{prop} \frac{u_i^2}{2} \\
 &+ \dot{m}_{prop} \frac{\vec{V}_{inj} \cdot \vec{V}_{inj}}{2} + \dot{m}_{prop} \left\{ h_{0(prop)} + \int_{T_{ref}}^{T_{inj}} C_{p(prop)} dT \right\} \\
 &- \dot{m}_w \sum_{l=1}^{n_{cs}} \alpha_{lw} [h_{il} - T_i s_l(T_i, P_i, \eta_{il})] \\
 &+ \dot{m}_i \sum_{l=1}^{n_{cs}} \alpha_{li} [h_{il} - T_i s_l(T_i, P_i, \eta_{li})] \\
 &- T_i (\dot{S}_{veh} + \dot{S}_{wake} + \dot{S}_{inj})
 \end{aligned} \quad (1)$$

In this equation, the left-hand side represents the vehicle (net) axial force-power (in the direction of vehicle movement). The first and second term on the right-hand side represent the overall (net) energy rates added as heat and work from the vehicle into the flow-path(s) associated with the global streamtube; the third term the kinetic energy rate associated with the injected propellant; the fourth and fifth term inclusively the total enthalpy rate associated with propellant injection; while the sixth and seventh term represent the change in chemical potential across the global streamtube from inlet (i) to equilibrated wake exit plane (w). Finally, the last (8th) term on the right hand side of Eq. (1) is the lost work associated with a) all entropy generation or transferred from the vehicle in and around the vehicle (from station i

to station e) (\dot{S}_{veh}), b) entropy generation in the unconstrained wake process (from station e to station w) (\dot{S}_{wake}), and c) entropy flow rate associated with injected propellant (\dot{S}_{inj}).

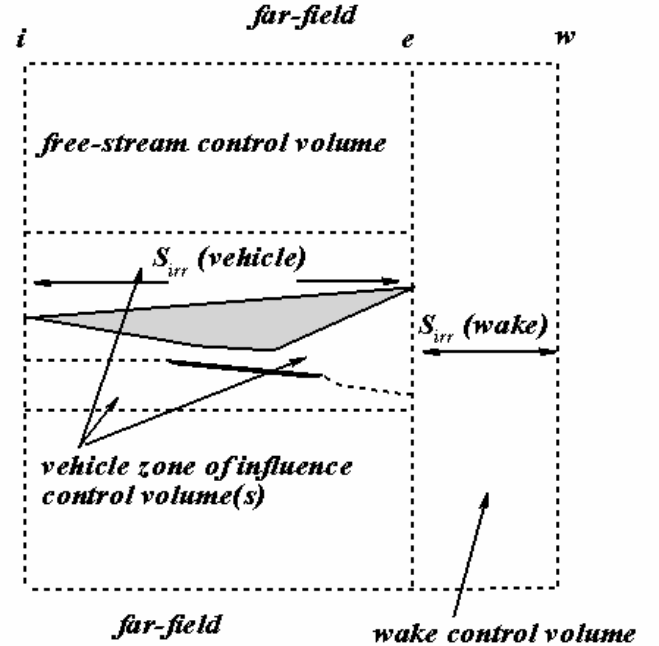


Fig. 2. Global streamtube for entropy-performance relationship (for use in Eq. (1))

This entropy – force relationship is also approximated very closely by the following relationship for a thermally balanced vehicle without (net) work interaction:

$$F_x \cdot u_i = \dot{Q}_{energetics} + \dot{m}_{prop} \left[\frac{u_i^2}{2} + H_{prop} \right] - T_i (\dot{S}_{irr-vehicle} + \dot{S}_{wake}) \quad (2)$$

In Eq. (2), the term H_{prop} is the heating value of the propellant and $\dot{S}_{irr-vehicle}$ is the entropy generation specifically due to irreversibilities occurring from i to e in the global streamtube. For both Eq. (1) and Eq. (2), the single-step analytical method for computing \dot{S}_{wake} is described in [2].

In the development of these relationships, the vehicle performance is therefore analyzed in terms of the fluid mechanics and thermodynamics of the global stream-tube which encompasses vehicle, near-field, the far-field and the wake region. The global stream-tube must be made large enough to realize the asymptotic limit inherent in the wake mixing process itself. Note that the following three important observations can be made by examining this particular relationship: 1) vehicle acceleration (or climb) really come down to ('just') overall entropy production due to irreversibilities and 2) there is no 'automatic' penalty for upstream injection or upstream heating – except as implicit in any irreversibility generated and 3) the complete description of the 'drivers' of vehicle performance in terms of entropy, energy, fuel characteristics, etc. can be thoroughly analyzed.

Specifically, Fig. 3 depicts a relevant question for high-speed vehicles involving the usage/management of on-board energy. Obviously, the second law analysis implicit in equation (1) and (2) are of great relevance to the challenge posed in this sketch. The following sections describe applications or scenarios relevant to this challenge and the entropic analysis (based on equation (1)) that assists in understanding results and relative performance.

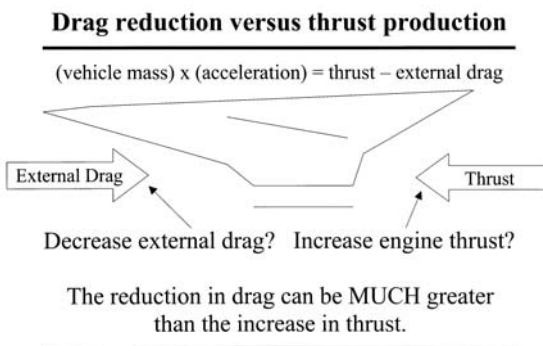


Fig. 3 Sketch of Aerodynamic Forces

3 Upstream Energy Deposition and Upstream-Directed Fluid Injection - Background

Many studies, both computational and experimental have shown the efficacy of upstream energy deposition for shock wave modification (and resulting drag reduction) on blunt bodies [20] – [24] as well as potential drag reductions for forward-facing upstream injection [25] – [31]. Forward facing injection from blunt bodies in high-speed flows when coupled with upstream deposition of energy has recently been shown to result in large decreases in overall drag and heat transfer [32]. The problem of upstream-directed injection jet instability has also been shown in this reference to be significantly reduced by the coupling of the two techniques (injection and upstream energy deposition); this allows the jet to penetrate far upstream and stabilize within bounds. When hydrogen is used as the core injectant, the substantial production of water in and near the zone of upstream energy deposition may assist in the efficiency of energy deposition systems. Additionally, by sheathing the hydrogen core with an inert injectant such as nitrogen, the body is cooled and the heat release and resulting zones of water production are removed from the vicinity of the blunt body. Cases have been shown in which the overall drag is only 20 to 30% of the base-line drag, heat transfer is minimal, and jet stabilization and forward penetration is ensured [32]. Figure 4 depicts a conceptual scenario of combined H₂/N₂ upstream injection with forward and localized (minimal) energy deposition.

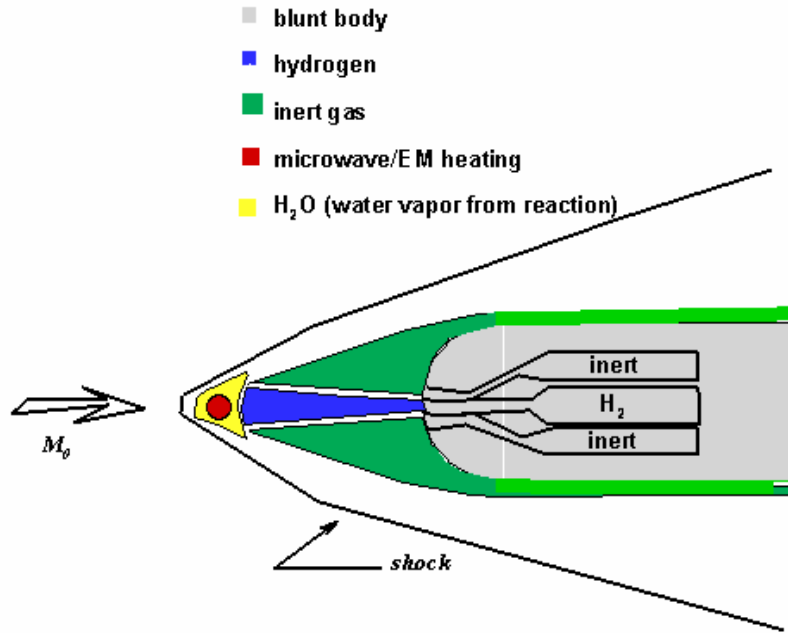


Fig. 4 Schematic of Forward Injection

Figure 5 shows the stabilization and drag reduction possible with forward-facing injection coupled with upstream energization as obtained in time-accurate CFD simulations for a representative blunt body in Mach 10 flight at 30 km altitude [32]. Here the drag reduction factor RD is defined as the ratio of drag for the flow-field modified utilizing injection and energy over the base-line (no flow-field modification) drag. RD includes the retro-rocket effect (drag component) due to forward jet injection itself. This figure initially provides RD versus iteration (or equivalently time for time-accurate CFD) for the case with both injection and energy deposition upstream without reaction. Drag reduction is seen to be very substantial – with drag stabilizing at around 25% of base-line. At a selected point in the time history, the injectant from the nose is reduced to zero, i.e. corresponding to the case with energization alone. Drag reduction is still good albeit there is less effect; flow-field modified drag is still approximately 55% of base-line. At the same point in the time history, a case is also simulated in which deposited energy is reduced to zero (but with injection

maintained). As can be seen in Fig. 5, the latter case with injectant alone collapses rapidly and yields very little drag reduction due to the instability of the injectant; it tends to fold against the body with little or no penetration forward. Also seen on this figure, is the fact that chemical reaction has little or no impact on the drag reduction achieved – nevertheless, the production of water in and around the zones of energy deposition may significantly improve the ability of candidate energization techniques such as micro-waves, etc. It should be noted that the power-based effectiveness of the technique is generally very high, i.e. if one defines power effectiveness as the drag power saved over the power input into the upstream flow, that effectiveness can reach extraordinarily high values (up to 60) for the given blunt body at high Mach numbers (6 to 10). Additionally, the amount of injectant (for these studies) is generally very small. However, it should also be noted that the large reductions of drag described here are directly related to the bluntness of the bodies examined, i.e. for such a configuration there is an inherent potential for significant drag reduction from the base-line.

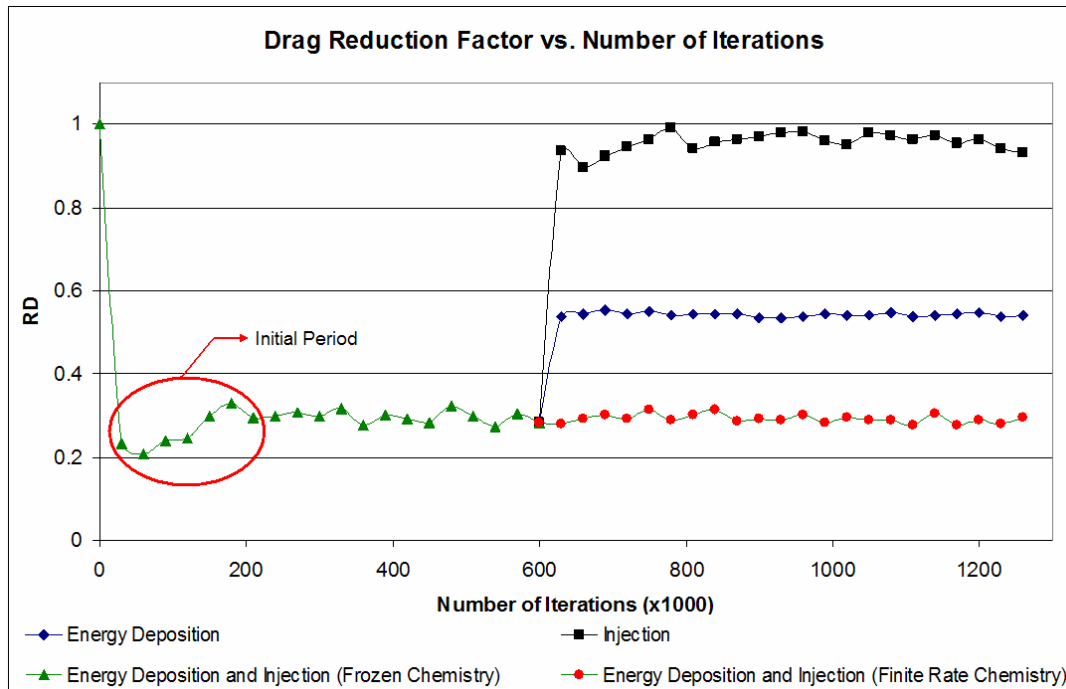


Fig. 5 Stability of Drag Reduction Factor (from [32])

4 Entropic Analysis of Blunt Body Drag Reduction Techniques

This section of the paper describes the second law characteristics as related to device force-based performance for a blunt-nosed two-dimensional body (same configuration as examined in [32] as discussed in the previous section) in Mach 10 flow in which drag reduction strategies utilizing upstream energy deposition and upstream-directed fluid injection are modeled. This body is essentially a wing-slab section with a hemispherical blunt nose followed by a constant area body and then truncating at the trailing edge to a sharp vertex as seen in the following plots. It is defined and treated here primarily as a test configuration for second-law concepts discussed earlier.

The CFD code used in this specific part of the study is a modified version of the 2D code SPARK, which was originally developed at NASA-Langley for use in studying internal reacting flow fields. Previous works have demonstrated the ability of the code to produce

reasonable results of the hypersonic blunt body problem. The code solves the laminar two-dimensional full Navier-Stokes equations by utilizing explicit time-marching. This allows time – dependent studies of unsteady or quasi-steady flow-fields and resulting flow-field development (as shown in the figure above). For the following cases, the walls are treated as adiabatic with no-slip velocity condition. Altitude corresponds to 30 km. The scale of the body is small with a slab thickness of only 1.5 cm. See Fig. 6 which depicts the two-dimensional grid for this configuration. The grid is defined by 601 points along the body from trailing edge (lower) to trailing edge (upper) and 151 points in the radial (outward from body surface) direction. Grid convergence issues have been addressed in previous work for similarly sized configurations (see [32]). Drag results are driven primarily by shock pressurization, i.e. Euler effects; hence the results of this and related studies should be nominally applicable to larger configurations, at least in terms of the dominant shock wave

losses, drag reductions obtained, and power effectiveness observed.

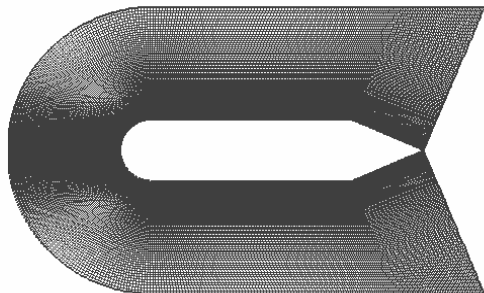


Fig. 6 Wing-slab grid for entropic analysis

Figures 7 through 9 depict pressure contours for three cases utilizing this blunt body at flight Mach number of 10. The first case is the baseline case (no injection and no energization). The second case is for upstream energization in a small zone located upstream of the body nose on body centerline. 100 kW of energy are deposited – the temperature in the deposition zone does not exceed 5000K. The third case is for a small amount of hydrogen sheathed with nitrogen injected upstream along with energy deposition at the same rate as the second case. As can be seen from these figures, the influence of the energy deposition on the shock wave by itself is dramatic in terms of weakening the bow shock (no longer normal but exceedingly oblique). Essentially the effective aerodynamic fineness ratio of the body has been significantly increased. The impact of upstream-directed injection along with the energy deposition is even greater in terms of weakening the shock structure. The injectant plume is stabilized and penetrates far forward even in this hypersonic Mach 10 stream as can be seen in Fig. 10 which shows hydrogen contours. Note that for these cases very small amounts of injectant are used.

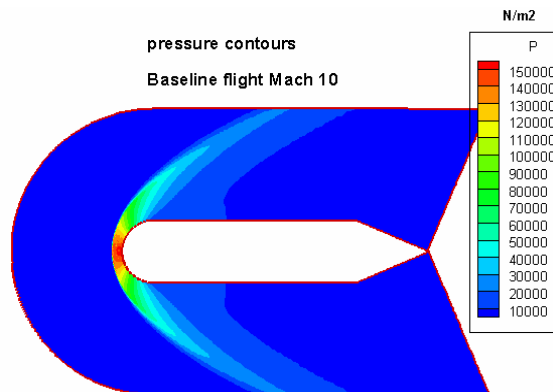


Fig. 7: Baseline Pressure Contours

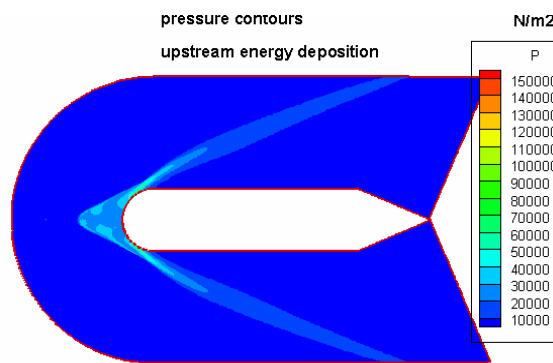


Fig. 8: Upstream Energy Addition Only Pressure Contours

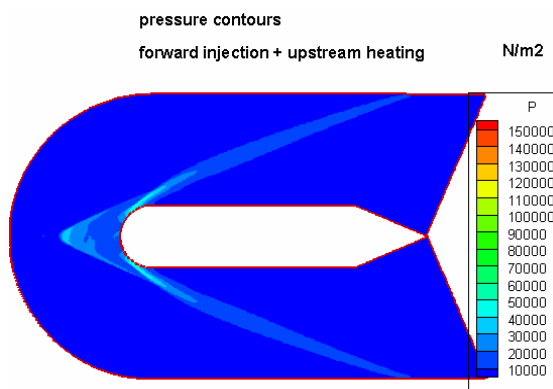


Fig. 9: Upstream Injection and Heating Pressure Contours

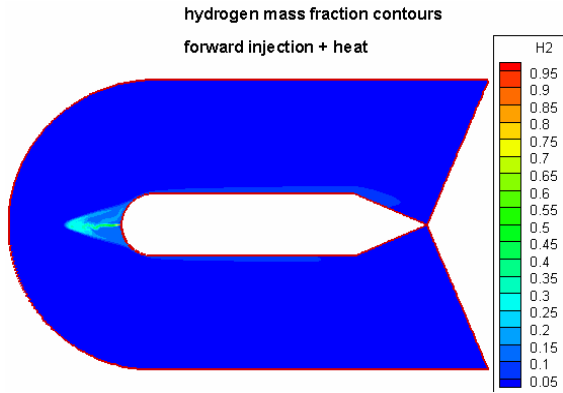


Fig. 10: Upstream Injection Hydrogen Mass Fraction Contours

Figures 11 thru 13 show entropy generation contours for these three cases; baseline, energy deposition alone, and energy deposition and forward injection. The entropy generation was obtained by extracting the net generation of entropy in each CFD cell – this was done by simply computing the net efflux per second of entropy out of that cell. It should be noted, however, that a mass flow rate correction was applied for each cell in order to account for unsteady effects so these graphical results (Fig. 11 – 13) are somewhat qualitative. The net entropy generation integrated across the flow-field in this manner has about 10% error when net exit plane entropy flow rates are calculated. This is attributed partially to numerical and modeling issues but primarily to low level unsteadiness inevitably associated with upstream injection as modeled in a time-accurate Navier-Stokes CFD code. The entropy generation for the base-line case is very large and the shock wave dominates the entropy production, as it should. It should be noted that the entropy production is highest in the normal shock region upstream of the centerline of the blunt nose but the shock layer is very thin there – it then tends to diffuse rapidly and spread as the shock progresses over the shoulders of the blunt body.

The entropy generation contours for the case with energy deposition alone shows dramatically reduced entropy generation associated with the weakening of the upstream shock structure; similarly the entropy generation

contours for the case with coupled injection/energy deposition shows similar small entropy production. The small far-upstream region of entropy production associated with the upstream heat addition is clearly evident in these figures.

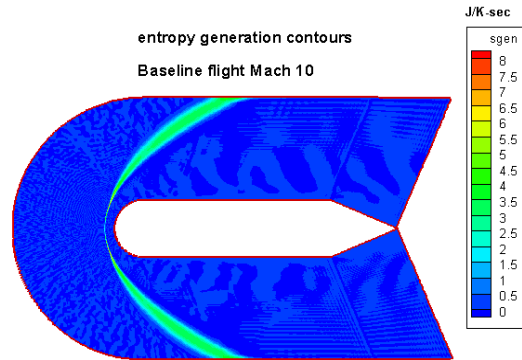


Fig. 11 Baseline Entropy Generation

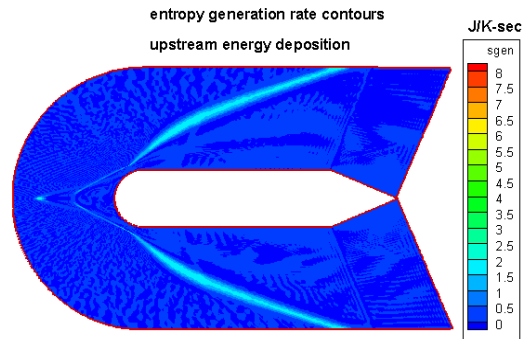


Fig.12 Upstream Energy Addition Entropy Generation

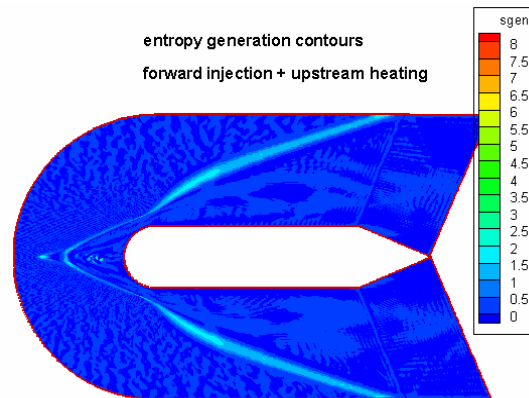


Fig. 13 Upstream Injection and Energy Addition Entropy Generation.

The following bar chart (Fig. 14) shows drag for the three configurations computed in three different manners: 1) integrated body pressures and shear-forces, 2) exit plane integrated stream thrust minus the inflow stream thrust (Newton’s method for the flow), and 3) utilizing the entropy method as described earlier (directly from Eq. (1)). In this case, because the configurations have fluid injection and are not (necessarily) thermally balanced, the general relationship between force production and entropy detailed in Eq. (1) is used rather than Eq. (2).

As can be seen, the agreement in computed drag between the three methods for each case is excellent; furthermore, the drag reduction is very large for both forward heat alone and even larger for forward heat plus injection. Keep in mind that the production of water potentially may assist drag reduction techniques. The comparisons of the computed drag for all configurations provide an excellent endorsement of the entropy method – particularly due to the explicit *entropy functional relationship* present in this method (i.e. potentially allowing a direct assessment of losses in terms of the *common currency* of entropy generation).

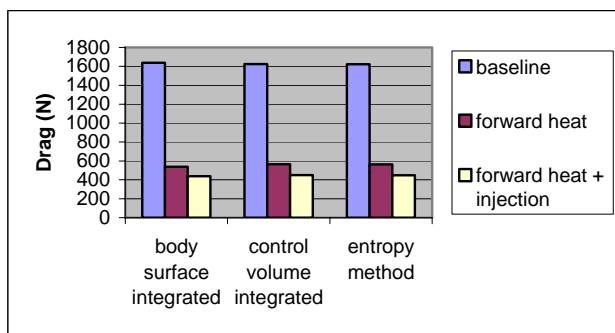


Fig. 14 Comparison of Drag Calculations using Three Methods

The following bar chart (Fig. 15) shows entropy rates due to irreversibility for these flow-fields; the entropy generated is sub-divided into both body control volume (out to the exit

plane of the body) and wake entropy production. Note that the base-line has much larger entropy production both over the vehicle and particularly in the wake, indicating a high degree of flow turning and non-uniformity at the exit plane of the body. Furthermore, for all cases, the wake entropy generation is much larger than irreversibilities occurring over the body; this has been observed to be absolutely typical of high-speed configurations in general.

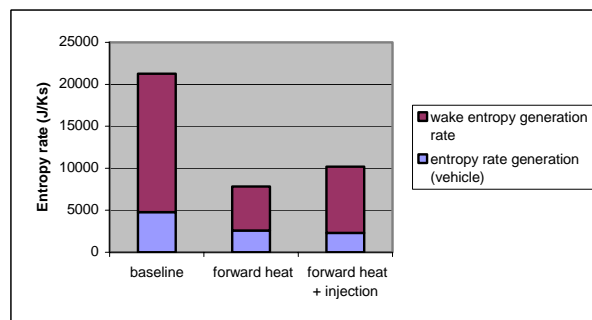


Fig. 15 Entropy Generation Rate

The following bar chart (Fig. 16) provides an assessment of the relative balance of the terms in the force power versus entropy equation (Eq. (1)) above. Note that the drag power is simply equal to the lost work rate due to irreversibility for the base-line case since there is no injection or upstream energy deposition. For the case of energy added upstream (no injection), the sum of the lost work rate due to irreversibility (negative) and the added energy (positive) yields the drag power. Finally, for the case with energy upstream and upstream injection, the sum of the lost work rate due to irreversibility, the added energy, and the change in Gibbs energy due to the chemical potential of the injectant with the environment is equal to the drag power. Even though the lost work term in this case is significantly larger than for the case with energy deposition alone, the Gibbs term (chemical potential of the injectant) more than makes up for that effect such that the net drag power is below that of the case with energy alone.

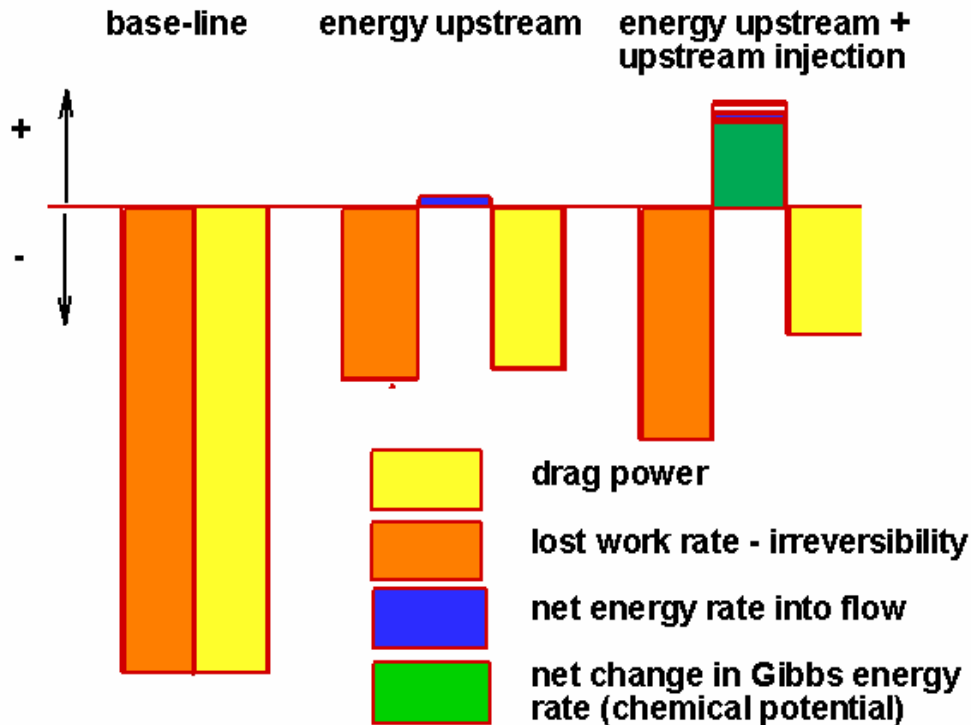


Fig.16 Force Power vs Entropy Generation (Contributions of terms – Eq. (1))

A tangential but important question is the actual cost of the drag reduction methodology in terms of the effectiveness of the technique (here neglecting transmission losses and system losses and weights), i.e. “*What are the ‘cost’ and effectiveness of the flow-field modification techniques?*”

The tabulation below summarizes the power characteristics for the previous two flow-modification cases as measured using the baseline (no flow modification). Note that the drag power reduction is the drag savings (from baseline to modified case) multiplied by the flight velocity (here 3000 m/s). This represents the reduction in required thrust power that an engine would have to provide due to the drag reduction – which translates more or less directly into a reduction in fuel consumed. So, for instance, if one J/sec of energy deposited upstream into the flow saves 10 J/sec of drag power – i.e. thrust power required - as measured from the base-line (no flow-field modification),

the power effectiveness of the technique is equal to 10.

Table 1: Upstream energy deposition alone:

Drag reduction (under base-line) = 1101 N
 Drag power reduction = 3.35 MW
 Power deposited in flow (on-board cost) = 0.1 MW

Overall power effectiveness = 33.5

Table 2: Upstream energy deposition with forward-facing injection (H₂ core/N₂ sheath)

Drag reduction (under base-line) = 1199 N
 Drag power reduction = 3.65 MW
 Power deposited in flow (partial on-board cost) = 0.1 MW

Injectant momentum drag = 31 N
 H₂ combustor heat rate potential = 0.74 MW
 H₂ (combusted) thrust power loss = 0.37 MW

Overall power effectiveness = 7.8

Although the power effectiveness of the energy deposition alone case is much higher than the case for simultaneous energy and injectant, the possible benefits of the injection must be kept in mind; these benefits include H₂O production in vicinity of upstream energy deposition, potential large reduction in upstream energy required, and cooling of the body surface, i.e. a tradeoff is possible and would be demanded for ‘energy management optimization’.

5 Coupling of Propulsion system with blunt body

As a simple but conceptually appealing example of the possible benefits of energy deposition and/or injection (or other energization methodologies) in a high-speed flow along with the related study of the fundamental second law characteristics of the situation, the same basic configuration is now taken and a rocket engine is ‘embedded’ within the device itself such that the base is now flat (corresponding to the exit area of the rocket nozzle) rather than tapering to a point as in the last section. This provides thrust which counters the drag associated with the configuration. This is done here in order to provide cruise at the indicated Mach number. The system energy requirements (the ‘energy balance’ between combustor and external flow-field) can then be studied in terms of both second law characteristics and optimization (i.e. finding the optimal energy or minimum propellant “design point”). This challenge is illustrated in Fig. 17 below. For this part of the study with an integrated propulsion system, only upstream energy is deposited, i.e. forward-facing injection is not used.

Specifically, a H₂-O₂ rocket engine is modeled within the body as shown; modeling assumptions are equilibrium kinetics and isentropic flow in the nozzle. The nozzle exit plane is coincident with the aft plane of the device. The rocket engine thrust is then matched to the external drag by throttling the fuel and oxidizer flow rate into the rocket combustion chamber. The purpose of the study is to show in a general sense that optimal (minimal) power requirements correlate with minimum entropy. As part of a related study, a number of parametric cases with varying upstream energy amounts, locations, and energy zone features were modeled and analyzed. These results are closely clustered in terms of configuration examined and actual results for the purposes of the present work and hence averaged results are used for ‘energized’ cases in order to show the relationship of entropy production to vehicle performance and optimization in terms of energy (fuel usage) management.

The following bar chart (Fig. 18) provides the overall onboard energy (or energy equivalent for H₂-O₂ propellant) required to cruise this ‘vehicle’ at Mach 10 for the baseline case (no modification or upstream energy) and for the average of five modified (upstream deposition of energy – labeled ‘forward energy’) cases. Note that the values for these five cases are tightly clustered in terms of achieved drag reduction, power effectiveness, and energy characteristics; for this reason, they are simply averaged to obtain an overall value. The overall onboard energy requirement for the base-line case is over three times that of the modified cases; also the amount of energy deposited forward is extremely small compared to the energy required in the combustor.

Find minimum overall power requirements required to cruise

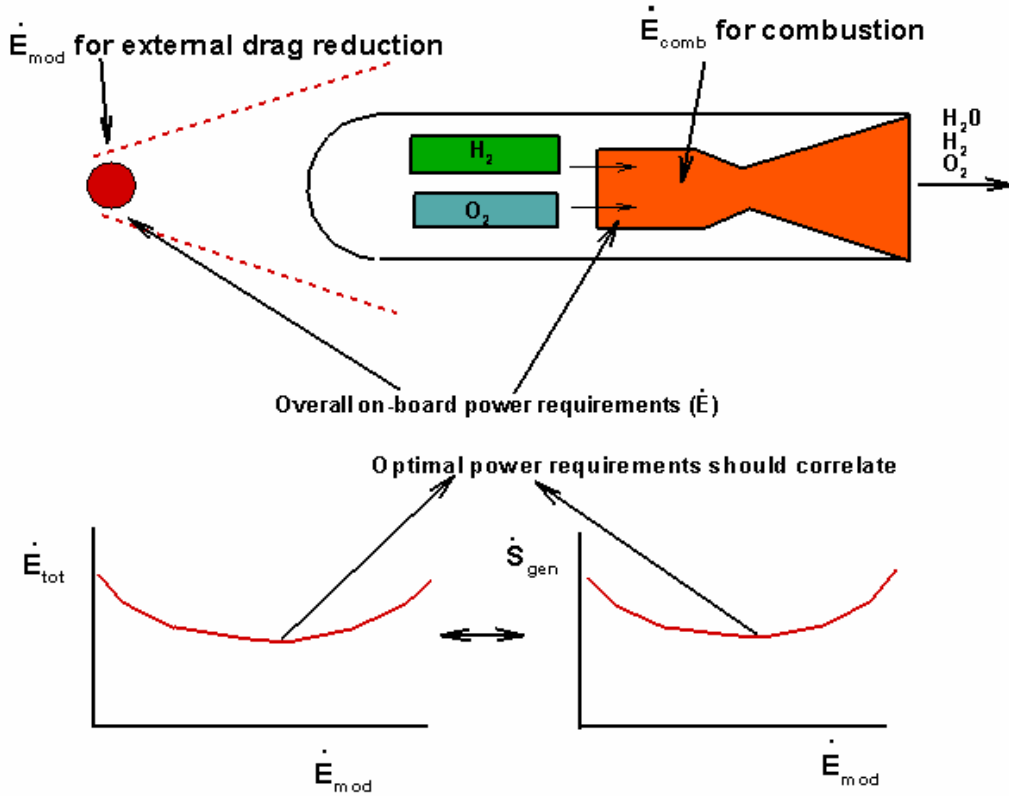


Fig. 17 Power Requirements for Cruise Condition

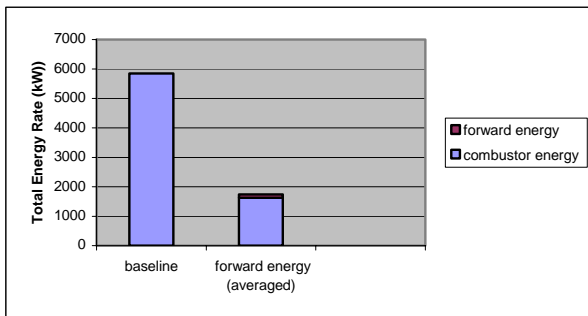


Fig. 18 Total Energy Rate Comparison for Simplified Thrusting Vehicle

Figure 19 shows the actual propellant usage in the rocket for both base-line and for the flow-modified cases. The propellant usage in the combustor is essentially equivalent to the

overall energy requirement since the energy deposited upstream is negligible compared to the energy usage in the combustor.

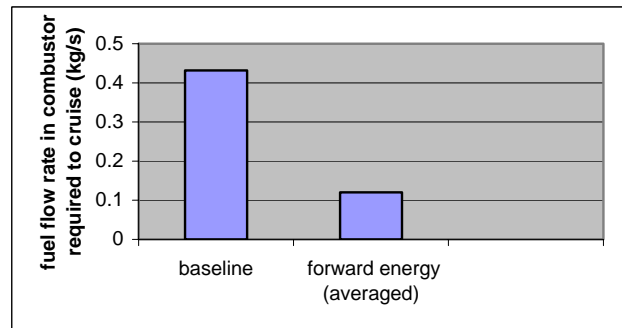


Fig. 19 Comparison of Fuel Flow Rate for Simplified Thrusting Vehicle

The bar chart below (Fig. 20) shows the overall production of entropy due to

irreversibility over the vehicle and in the wake for the baseline and the averaged forward energy cases. Note that in these cases (as in all high-speed cases investigated thus far), the wake entropy production is very large and is clearly dominant for the cases with flow-field modification. This is primarily due to the much smaller entropy production in the vehicle flow-field as the wake entropy rates are very similar between the base-line and the upstream energized cases.

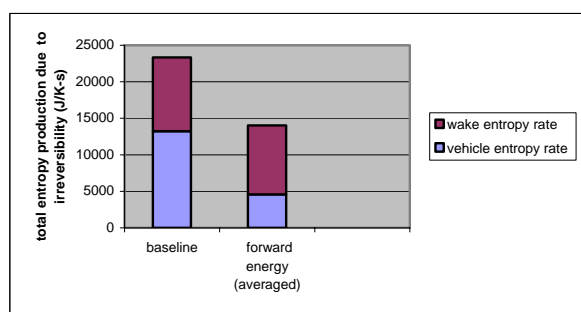


Fig. 20 Comparison of Entropy Production Rates for Simplified Thrusting Vehicle

6 Full Vehicle Study – energy distribution between aero/propulsion flowpaths

The following sections detail an investigation regarding the effective use of on-board energy on a full (2-D) ‘generic’ hypersonic vehicle. This investigation focused on the utilization of a fixed amount of available energy and its ‘appropriate distribution’ between propulsion and aerodynamic locations for maximizing force-based performance of the vehicle. In this study, all energy ‘sources’ were simply modeled utilizing heating source terms within the energy equation and distributed spatially within the component or region identified, including in the combustor. This was deemed sufficient for the purpose of this study which was to demonstrate in broad terms the potential for increased performance through the distribution of energy in and around a hypersonic vehicle and to perform the related second-law analysis on configurations of interest. Since this process involved a parametric study with numerous

possible trial configurations (amount and location of energy input), a standard statistical software package was used to define an appropriate set of cases for analysis. This statistical analysis resulted in the definition of ten cases (or configurations) for computation. Based on previous experience with similar configurations, the maximum amount of energy addition for deposition in the upstream was set at 200 kW. The maximum amount of energy used to increase mass capture (energy added slightly upstream and below cowl leading edge) was 150 kW and the remainder (the bulk) of baseline ‘stoichiometric’ energy was deposited into the combustor.

6.1 VULCAN CFD Code Description

The CFD code used for all simulations in the section was VULCAN version 5.0.0, developed at NASA Langley. This CFD tool solves the full, viscous Navier-Stokes equations, and uses a k-omega turbulence model with the Menter Shear Stress Transport model modification. Triple interval curve fits which are valid through 20,000 K are used for thermodynamics. Since the 2-D vehicle used simple energy addition as a model for exothermic heat release associated with fuel addition, no fuel-air finite rate chemical kinetics model was used in this study. However, since temperature of the air in and around the vehicle reached very high values, an air-dissociation chemistry model incorporating N₂, O₂, N, O, and NO was used.

All studies utilizing VULCAN were conducted using an 18 node computer cluster located at the University of Missouri-Rolla. VULCAN was installed for use in parallel mode such that the overall grid for the flow domain is distributed individually across processors.

6.2 Grid Used for Generic Hypersonic Vehicle and Boundary Conditions

The 2-D grid used to generate the specific results presented in this part of the study is shown in Fig. 21. This grid is composed of 18 blocks; each block is each associated with an individual processor.

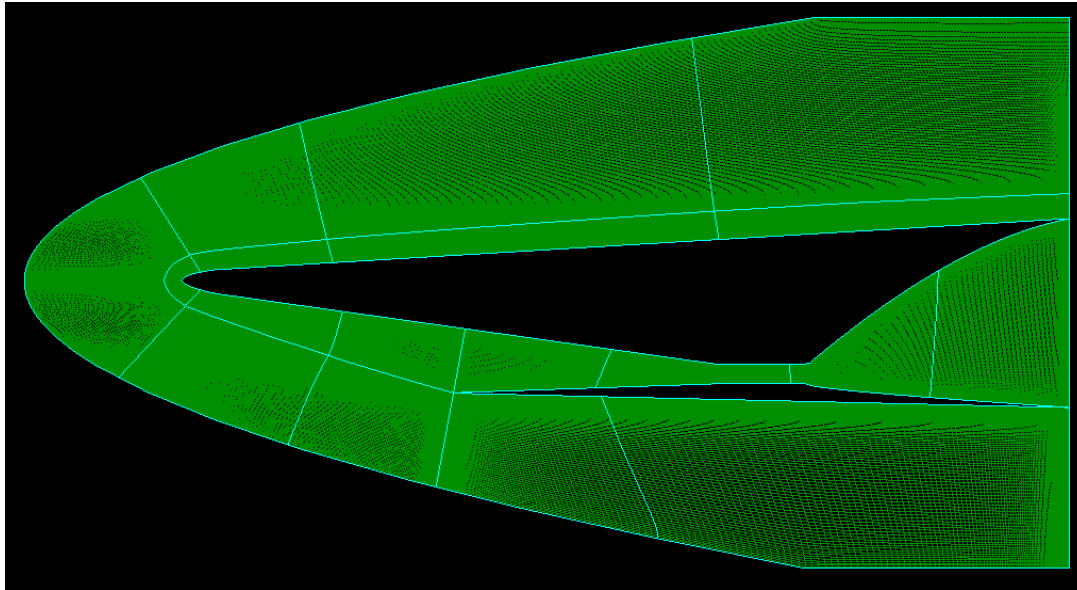


Fig. 21 2-D vehicle grid

The vehicle is sub-scale as shown with an overall nose-to-tail dimension of 0.30 meters. The upstream energy deposition zone was located between 5.3 cm and 3.6 cm upstream of the vehicle nose ($x = 0$) with a spatial aspect ratio (length to height) of 2.87. The forward-of-cowl energy deposition zone was located between 1.57 cm and 1.11 cm upstream of the cowl leading edge and centered vertically .183 cm below the leading edge with aspect ratio of 6.56. Since these energized zones simply followed the grid, they are essentially rectangular. Energy is simply added in the combustor in a block region from 0.1 cm downstream from combustor shoulder to 0.6 cm upstream of combustor exit (and 0.04 cm from top and bottom combustor walls). The nose of the vehicle is slightly blunted as compared to a typical configuration in order to better facilitate flow-field (upstream shock-wave) modification using energy methods. A constant area heat addition region models the vehicle combustor. Vehicle wetted surface temperatures were kept

constant at 800K and inflow conditions used corresponded to flight Mach 10 and 30 km altitude.

6.3 Results of Distributed Energy Study for Generic Hypersonic Vehicle

Table 3 provides a summary of results obtained in this study. There are a total of ten cases shown in this table. Note that each case has a different distribution of energy between locations upstream of vehicle nose, upstream and below cowl leading edge, and in the combustor. However, in all cases with energy addition, the amounts of deposited energy associated with locations upstream of vehicle nose and below the cowl are seen to be extremely small as compared with the energy associated with the combustor.

Table 3: Experimental Set Results for Distributed Energy for Hypersonic Vehicle

Case	Location/Energy Addition (kW)			Qwall	%mdot	Fx Wall	Fx	Fx
	Upstream	Cowl	Comb					

				(kW)	Inc.	(N)	Stream (N)	Entropy (N)
NoHeat	0	0	0	755.1	0.00	-967.6	-977	-977
AllComb	0	0	7296	1537.4	0.44	-210.7	-230	-230
MaxThrust	100	75	7121	1047.5	2.06	296.3	291	291
c2	0	150	7146	1528.2	3.81	-200.3	-221	-221
c3	200	0	7096	1236.5	-0.77	35.3	45	45
c4	200	150	6946	1193.5	2.68	121.1	127	127
c6	50	37.5	7208.5	1061.6	1.26	116.7	108	108
c7	50	112.5	7133.5	1065.9	2.69	127.1	118	118
c8	150	37.5	7108.5	1185.8	0.93	55.4	73	73
c9	150	112.5	7033.5	1186.8	2.30	84.7	101	102

Case	Location/Energy (kW)			Addition J/K-sec S veh	J/K-sec S wake	Watts Q net	J/K-sec S total
	Upstream	Cowl	Comb				
NoHeat	0	0	0	3074	6188	-820.4	9262
AllComb	0	0	7296	5580	21306	5573.8	26886
MaxThrust	100	75	7121	4777	17061	5987.9	21838
c2	0	150	7146	5698	21076	5573.6	26774
c3	200	0	7096	4626	19638	5801.0	24264
c4	200	150	6946	4780	18862	5905.1	23642
c6	50	37.5	7208.5	4976	19465	6035.9	24441
c7	50	112.5	7133.5	5002	19268	6026.6	24270
c8	150	37.5	7108.5	4754	19698	5929.8	24452
c9	150	112.5	7033.5	4784	19358	5945.1	24142

The first three cases listed in this Table provide the main results of interest here and correspond to a) the 'NoHeat' case which is for no energy at all in or around the vehicle, b) the 'AllComb' case which is for all energy put into combustor, and c) the 'MaxThrust' case which is the specific configuration ('balance' of energy) in this study that yielded the maximum axial (accelerative) force. The remaining seven cases listed in Table 3 have been identified with a given alpha-numeric designation. Note that a positive F_x indicates a net accelerative force on the vehicle while a negative value for this quantity indicates a net deceleration force on the vehicle. The effect of the cowl-side energy deposition for increasing mass capture is smaller in terms of providing overall performance enhancement than energy added upstream of the vehicle. The data can be directly examined for other trends and it is found (for example) that the optimal amount of energy to be added upstream can be estimated as slightly over 100 kW. Since the Q_{wall} column in the table is the overall heat transfer rate to

vehicle wetted surfaces, it can be seen that not only does upstream energy addition substantially increase the net axial force experienced by the vehicle, it actually can have potential in reduction of the overall heat transfer experienced by the vehicle.

Also shown in Table 3 is the actual net axial force in Newtons experienced by the vehicle (F_x) as computed using three techniques: a) integrated pressure and shear forces on vehicle wetted surfaces (F_{xwall}), b) nose to tail control volume momentum (stream thrust) calculation ($F_{xstream}$), and c) entropy method as computed using Eq. (1), $F_{xentropy}$. The relatively minor differences between the wall integration results and the other two methods are attributed to numerical (algorithmic) and grid resolution issues. Note, however, that the net axial force found from overall change in stream thrust through the control volume encompassing the vehicle is almost exactly duplicated by the axial force found using the entropy method.

6.4 Comparative Flow-Field Description

Fig. 22 shows flow-field results for the case where all available energy was added in the combustor alone, therefore representing a ‘conventional’ vehicle design (termed ‘AllComb’ case). Here the total pressure

contours (top) show typical shock structures in the inlet and above the vehicle; the axial (U) velocity contours (bottom) clearly depict the initial deceleration in inlet (due to area constriction) and combustor (due to heat release) and the subsequent flow expansion through the nozzle.

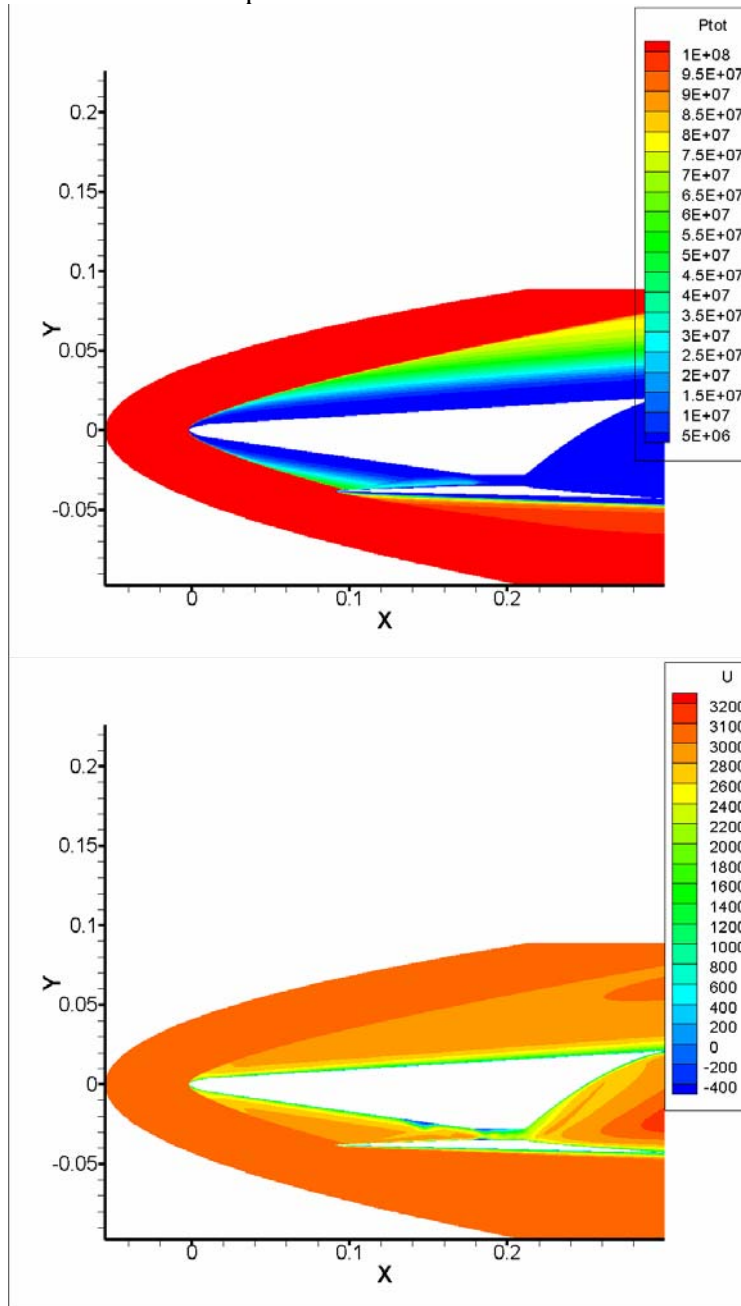


Fig. 22 AllComb - Total Pressure contours on top, U velocity contours on bottom.

Fig. 23 shows the same contours for the case with the specific distribution of the energy between combustor, cowl, and upstream in which the maximum axial force was produced (termed 'MaxThrust' case). For this maximum performance case, the total pressure contours in

this figure show the effect of the energy addition upstream of the nose and in front of and below the bottom cowl. It can also be seen that the inlet shock is much weaker due to the upstream energy addition and there is increased expansion in the nozzle.

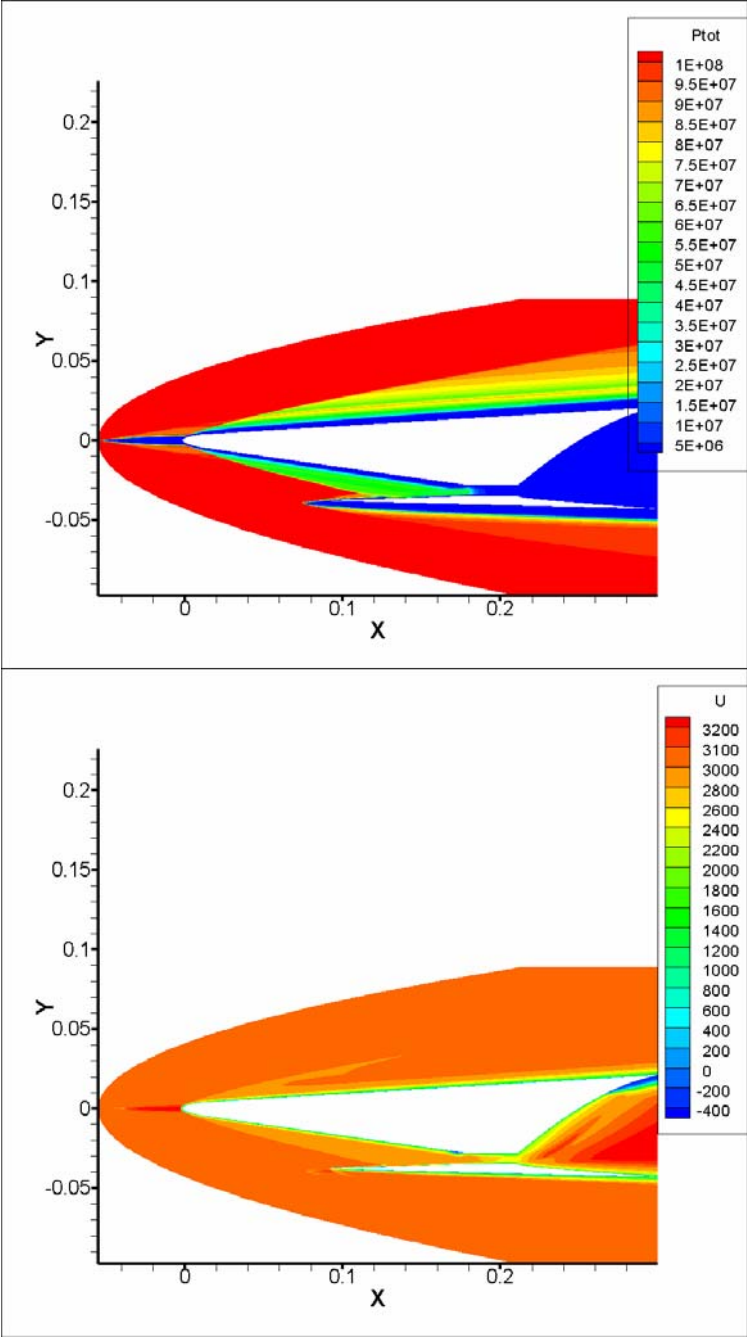


Fig. 23 MaxThrust case - Total Pressure contours on top, U velocity contours on bottom.

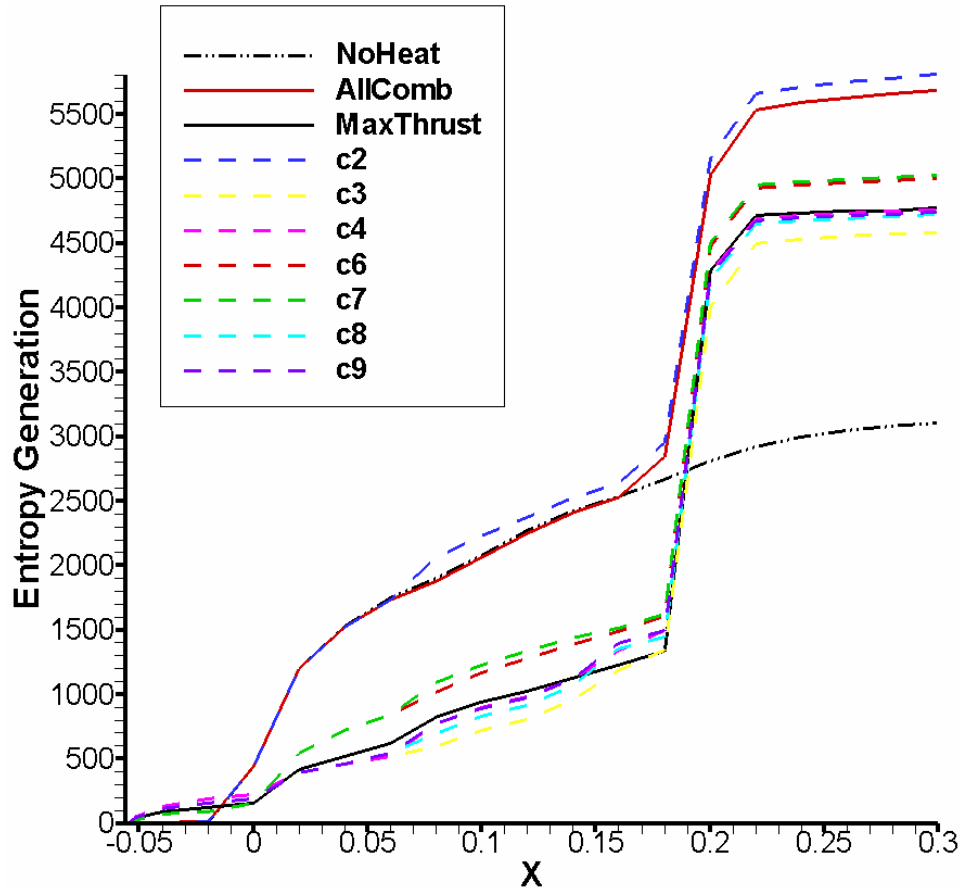


Fig. 24 Entropy Generation from freestream to exit of vehicle.

6.5 Entropy Distributions for Full Vehicle Cases

Figure 24 is a plot of entropy generation distribution from the free-stream inlet plane to the exit plane of the vehicle. All cases listed in Table 3 are plotted in this figure.

The entropy generation upstream of the vehicle for cases with upstream energy deposition can be seen in this figure (note rise in entropy for relevant cases upstream of the nose of the vehicle). However, for the cases with energy deposition upstream of the vehicle, the entropy generation in the inlet is considerably less due to weaker shock wave structures (both incident and reflected) in the inlet. Conversely, the entropy generation through the combustor (entrance located approximately at 0.18 m) is also seen to be somewhat increased for the cases with significant upstream addition of energy due

to the weaker inlet shock system. This is expected since the combustor Mach numbers will be higher for the weaker inlet shock structure (less compression), which will then cause more entropy production due to Rayleigh (heat addition) losses in the combustor. The other important observation is that the maximum thrust case is not seen to have the lowest entropy generation when measured from vehicle nose to tail (to the indicated exit plane of the vehicle). Also notice that the case designated as c2, which had slightly better axial force performance than the AllComb case (i.e. the case with all energy put into the combustor) nevertheless has a higher entropy generation from vehicle nose to vehicle exit plane. For correspondence between entropy generation and vehicle performance utilizing the methods discussed in this work, it is therefore necessary to include the entropy generation due to the wake generation in the second-law analysis in

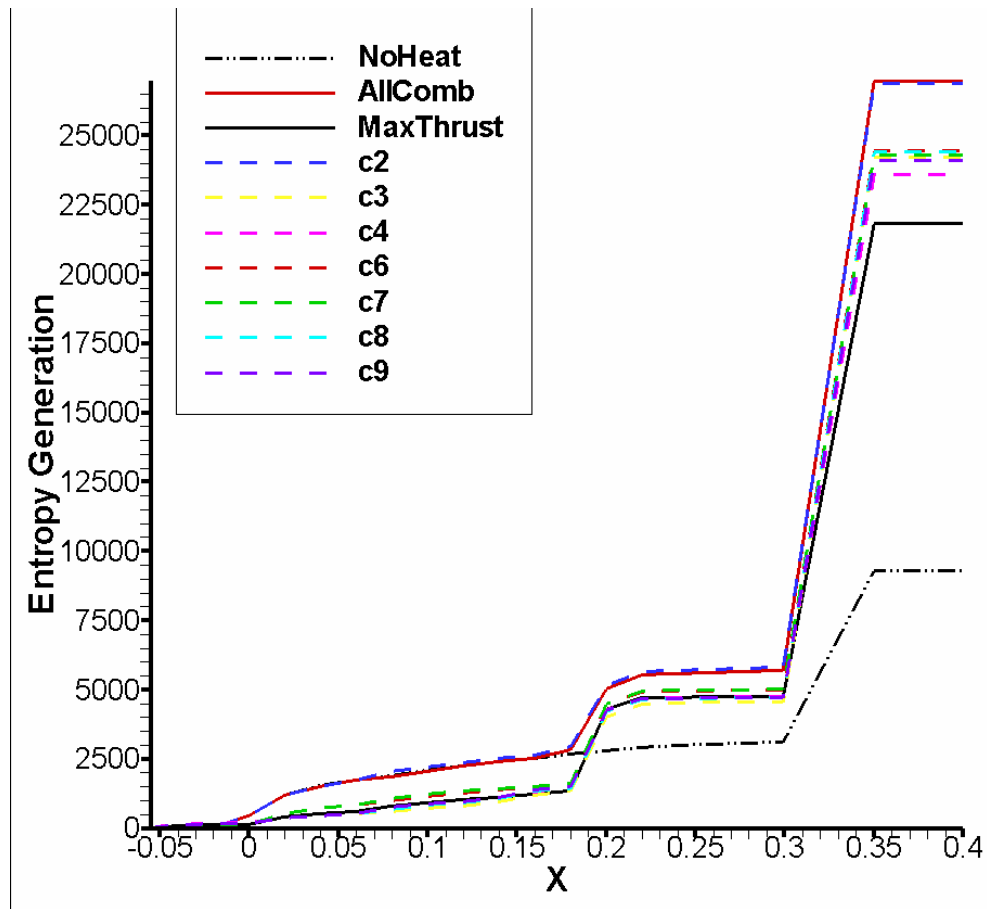


Fig. 25 Entropy Generation from freestream to vehicle exit, plus wake mixing.

order to accurately analyze the forces on a hypersonic vehicle. Figure 25 includes the wake mixing entropy gain as computed from methodologies discussed in earlier sections of this paper. For ease of plotting, the wake entropy generation is simply added to the cumulative entropy distribution as a linear ramp from vehicle exit plane (at $x = .3$) to $.35m$ and then shown as constant from $.35$ to $.4m$ in order to illustrate the value of the final overall entropy generation. The locations of $.35m$ and $0.4m$ are arbitrarily chosen.

With the inclusion of the wake equilibration process, the maximum thrust case has the lowest overall entropy generation (which is mandated by the entropy analysis). Also, case (c2) now has a slightly smaller entropy generation than the AllComb case which also corresponds with force-based performance observed. However, note that the rest of the cases, which have very similar axial forces (i.e. cluster very closely), do not all exactly line up in terms of lower overall

entropy production correlating to higher (productive) axial force. This is due to the fact that the entropy audit as described in Eq. (1) includes the wall heat transfer as a contributing term in the balance. When the heat transfer rates are included, the correspondence is indeed correct (see Table 3).

The summary bar charts (Figures 26 and 27) shown below illustrate the concepts discussed above and in earlier sections for the three basic cases (no heat in flowpath, all heat in combustor, and maximum axial force case). Shown are the net axial force on the vehicle as computed using body force integration techniques (pressure and shear), overall control volume integrated stream thrusts, and the entropy method. Also shown in the second bar chart is the entropy production. The dominance of the irreversibility in the vehicle wake is plainly seen; note that this corresponds to a very non-equilibrium situation at the vehicle exit plane as discussed earlier in this paper.

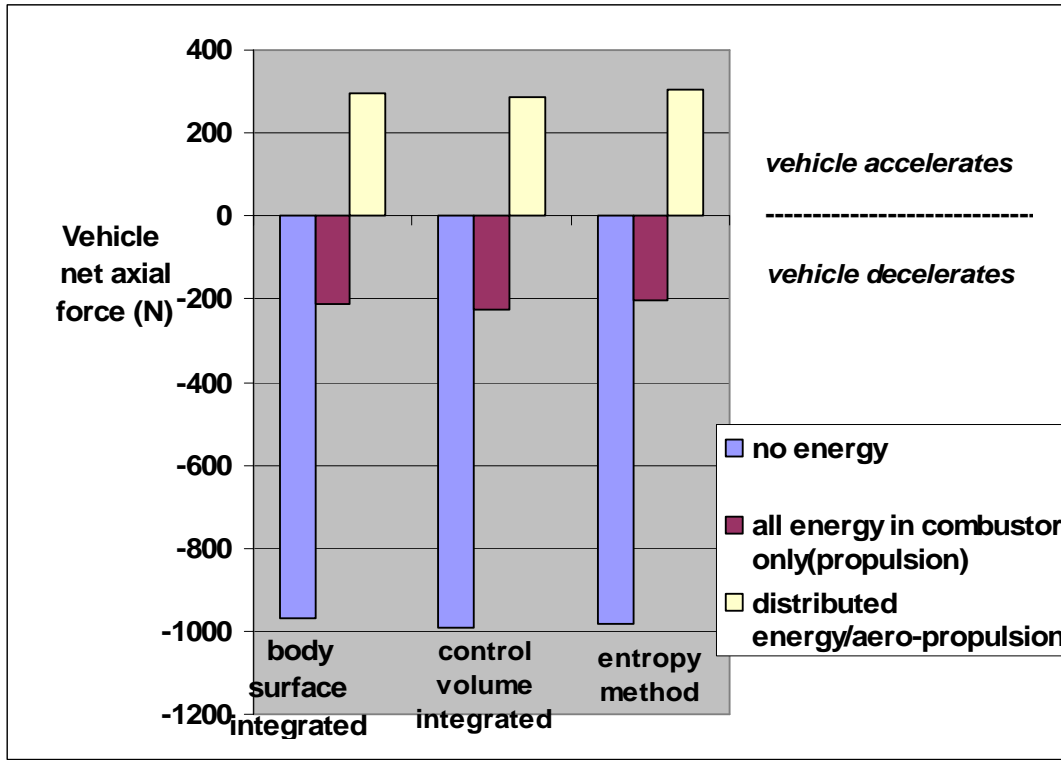


Fig. 26 Net Axial Force Summary (Full Vehicle Study)

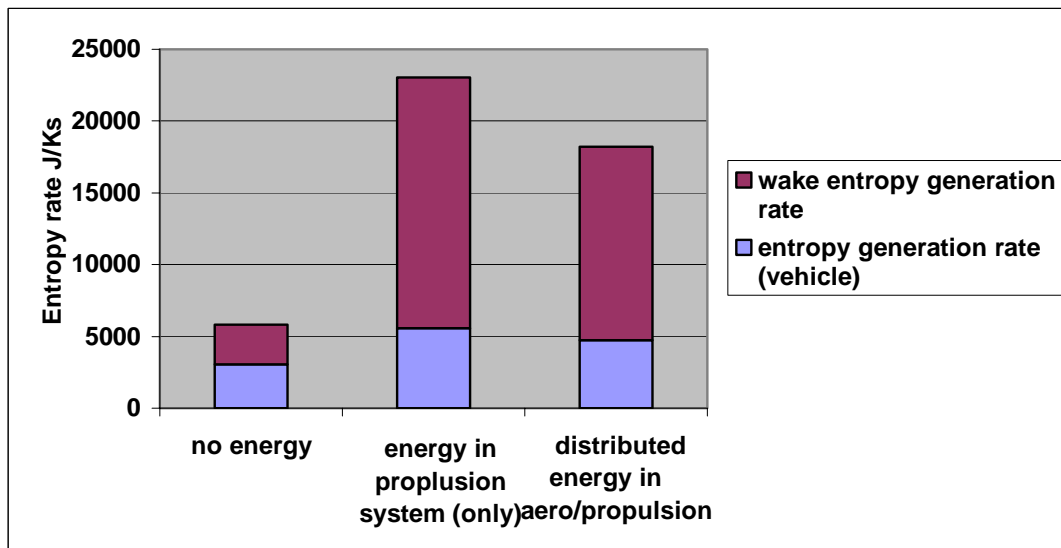


Fig. 27 Entropy Generation Rate Summary (Full Vehicle Study)

7 Conclusions

This analytical and numerical investigation provides applications and studies relevant to the vehicle performance-entropy relationship derived and examined in previous studies. This relationship provides the direct quantitative correspondence between vehicle energy management, entropy production due to irreversibility in both vehicle flow-field (aerodynamic and propulsive) and vehicle wake, and vehicle performance. The applications discussed here which utilize this relationship focus (in this paper) on cases with on-board energy distributed in the external aerodynamic flow-field as well as in the propulsive flow-path of hypersonic shapes and vehicles. Specifically, a simplified configuration of a two-dimensional blunt body at high Mach number is examined utilizing a Navier-Stokes CFD code for cases with forward-facing injection and forward-facing injection with upstream energy deposition (as heat); these are compared with the base-line case. The entropy characteristics of the flow-fields for these cases are calculated; these characteristics clarify the relative performance of these cases and demonstrate the utility of the direct link between entropy generation and vehicle performance for configuration analysis, design and optimization. This concept is then coupled with a simplified rocket-based (H₂-O₂) propulsion system in order to clearly demonstrate the direct relationship between propellant flow rate minimization and minimum overall entropy generation.

A second part of the investigation demonstrates the potential advantage of distributing energy in both external airstreams upstream and adjacent to an actual hypersonic vehicle configuration as well as in the 'traditional' location of the engine combustor. In this part of the investigation, entropy analysis has been performed on a number of entire vehicle flow-fields and the performance has been related to the generation of entropy due to flow irreversibilities in both the vehicle flow-field as well as in the vehicle wake. This has used the entropy –performance analysis

previously described. A tailored distribution of energy upstream of the vehicle and upstream and below the cowl leading edge serves as a powerful supplement to the combustor energy cost in terms of enhancing vehicle performance. Not considered here, however, are the system penalties that will be associated with the additional components required in order to achieve this energy deposition capability. However, since there is such a large performance margin achieved in terms of power effectiveness without any consideration of system penalty, it is believed that more study is necessary and that even relatively large system penalties may not be able to counter the performance advantage of the distributed energy concept. In a very real sense, a vehicle designed based on these principles would be a design that attempts to tailor the flow-field to 'fit' the vehicle shape, configuration, and constraints instead of tailoring the vehicle shape, etc. to 'fit' the flow-field (as is conventionally done). The vehicle designed in such a manner could (conceivably) be more structurally efficient (i.e. reduce actual fineness ratio while maintaining or even increasing *effective* aerodynamic fineness ratio), more volumetrically efficient, and more easily cooled for reusability and durability. Perhaps the largest benefit would be that the vehicle may be able to operate in a wide range of flight regimes since it may be able to actively and dynamically control the flow conditions that it is encountering.

The major purpose of this overall work was to develop, understand, and apply entropy production as criteria (ultimately 'the' criteria) in order to evaluate vehicle performance and performance losses consistently. This forms the basis for the use of a 'common currency' in the current vehicle design process – the use of energy concepts examined here are one example of where entropic analysis may be of great use. Such capability may allow the development of new and innovative concepts that do not 'just' marginally improve performance but may enable the realization of entire new regimes of performance and operability for high-speed aerospace vehicles.

Acknowledgements

The authors would like to thank Dr. Jose Camberos of the Air Force Research Laboratory. Thanks are due to the Air Force Office of Scientific Research for support under the auspices of the AFRL Summer Research Program during 2004, 2005 and 2006.

References

- [1] Moorhouse, D., "A Proposed System-Level Multidisciplinary Analysis Technique Based on Exergy Methods", *AIAA Journal of Aircraft*, Vol. 40, No. 1, 2003, pp. 10-15.
- [2] Riggins, D., Taylor, T., and Moorhouse, D., "The Second-Law Based Analysis of Aerospace Vehicle Performance", AIAA Paper 2006-0336, January 2006.
- [3] Foa, J., *Elements of Flight Propulsion*, Wiley and Sons, New York, 1960, Chapter 13.
- [4] Riggins, D.W., "The Thermodynamic Continuum of Jet Engine Performance; The Principle of Lost Work due to Irreversibility in Aerospace Systems", *International Journal of Thermodynamics*, Vol. 6, No. 3, 2003, pp. 107-120.
- [5] Lewis, J.H., "Propulsive Efficiency from an Energy Utilization Standpoint", *Journal of Aircraft*, Vol. 13, No. 4, 1976, pp. 299-302.
- [6] Curran, T. and Craig, R., "The Use of Stream Thrust Concepts for the Approximate Evaluation of Hypersonic Ramjet Engine Performance", USAF Aero-Propulsion Laboratory TR-73-38, 1978.
- [7] Riggins, D., McClinton, C.R., and Vitt, P., "Thrust Losses in Hypersonic Engines Part 1: Methodology", *AIAA Journal of Propulsion and Power*, Vol. 13, No. 2, 1997, pp. 281-287.
- [8] Riggins, D., "Thrust Losses in Hypersonic Engines Part 2: Applications", *AIAA Journal of Propulsion and Power*, Vol. 13, No. 2, 1997, pp. 288-295.
- [9] Roth, B., "Comparison of Thermodynamic Loss Models Suitable for Gas Turbine Propulsion", *AIAA Journal of Propulsion and Power*, Vol. 17, No. 2, 2001, pp. 324-332.
- [10] Roth, B., "A Work Potential Perspective of Engine Component Performance", *AIAA Journal of Propulsion and Power*, Vol. 18, No. 6, 2002, pp. 1183-1190.
- [11] Clarke, J., and Horlock, J., "Availability and Propulsion", *Journal of Mechanical Engineering Science*, Vol. 17, No. 4, 1975, pp. 223-232.
- [12] Czysz, P. and Murthy, S., "Energy Analysis of High-Speed Flight Systems", *High-Speed Flight Propulsion Systems*, edited by T. Curran and S. Murthy, Progress in Astronautics and Aeronautics, AIAA, Washington, D.C., 1991, pp. 143-236.
- [13] Riggins, D., "Evaluation of Performance Loss Methods for High-Speed Engines and Engine Components", *AIAA Journal of Propulsion and Power*, Vol. 13, No. 2, 1997, pp. 296-304.
- [14] Riggins, D., "High-Speed Engine/Component Performance Assessment Using Exergy and Thrust-Based Methods", NASA Contractor Report - 198271, 1996.
- [15] Oswatitsch, K., *Gas Dynamics*, Academic Press Inc., New York, 1956, Chap. 4.
- [16] Giles, M. and Cummings, R., "Wake Integration for Three-Dimensional Flowfield Computations: Theoretical Development", *AIAA Journal of Aircraft*, Vol. 36, No. 2, 1999, pp. 357-365.
- [17] Greene, G., "An Entropy Method for Induced Drag Minimization", SAE Technical Paper Series #892344, 1989.
- [18] Roth, B., "Aerodynamic Drag Loss Chargeability and its Implications in the Vehicle Design Process", AIAA Paper 2001-5236, Oct. 2001.
- [19] Roth, B. and Mavris, D., "A Generalized Model for Vehicle Thermodynamic Loss Management and Technology Concept Evaluation", SAE Paper 2000-01-5562, Oct. 2000.
- [20] Knight, D., "Survey of Aerodynamic Flow Control at High Speed by Energy Deposition," AIAA Paper No. 2003-0525, January, 2003.
- [21] Marconi, F., "An Investigation of Tailored Upstream Heating for Sonic Boom and Drag Reduction," AIAA Paper 98-0333, January 1998.

[22] Riggins, D. W., Nelson, H. F., and Johnson, E., "Blunt Body Wave Drag Reduction Using Focused Energy Deposition", AIAA Journal, Vol. 37, No. 4, 1998, pp. 460-504.

[23] Kogan, M., Ivanov, D., Shapiro, E., and Yegorov, I., "Local Heat Supply Influence on a Flow over a Sphere," AIAA Paper 2000-0209, January 2000.

[24] Taylor, T., "Drag Reduction and Control Using Energetics and Electrostatic Force-Fields for Hypersonic Applications", AIAA Paper 2004-0131, 2004.

[25] Charczenko, N. and Hennessey, K. W., "Investigation of a Retrorocket Exhausting From the Nose of a Blunt Body into a Supersonic Free Stream," NASA Technical Note D-751, September 1961.

[26] Meyer, B., Nelson, H. F., and Riggins, D. W., "Hypersonic Drag and Heat Transfer Reduction Using a Forward Facing Jet", AIAA 99-4880, November, 1999.

[27] Charwat, A. F., "Investigation of the Flow and Drag Due to Supersonic Jets Discharging Upstream into a Supersonic Flow," NASA Technical Report AD-603354, July 1964.

[28] Love, E. S., "The Effects of a Small Jet of Air Exhausting From the Nose of a Body of Revolution in Supersonic Flow," NACA Research Memorandum LL52I19a, November 1952.

[29] Romeo, D. J. and Sterrett, J. R., "Exploratory Investigation of the Effect of a Forward-Facing Jet on the Bow Shock of a Blunt Body in Mach 6 Free Stream," NASA Technical Note D-1605, February, 1963.

[30] Tolle, F. F., "An Investigation of the Influence of a Forward Ejected Gas Stream on Hypersonic Flow about Blunt Bodies", Dissertation at the University of Arizona, 1973.

[31] Finley, J. P., "The Flow of a Jet From a Body Opposing a Supersonic Free Stream," Journal of Fluid Mechanics, Vol. 26, part 2, October 1966, pp. 337-368.

[32] Taylor, T, Khamooshi, A., and Riggins, D., "Innovative Concepts for Large-Scale Drag and Heat Transfer Reductions in High-Speed Flows", AIAA Paper 2006-0660, January, 2006.